Published in final edited form as:

Cancer Res. 2018 June 15; 78(12): 3135–3146. doi:10.1158/0008-5472.CAN-17-3460.

SETD2 Haploinsufficiency for Microtubule Methylation is an Early Driver of Genomic Instability in Renal Cell Carcinoma

Yun-Chen Chiang[1], **In-Young Park**[2], **Esteban A. Terzo**[3], **Durga N. Tripathi**[2], **Frank M. Mason**[3], **Catherine C. Fahey**[1], **Menuka Karki**[2,4], **Charles B. Shuster**[4], **Bo-Hwa Sohn**[2], **Pratim Chowdhury**[2], **Reid T. Powell**[5], **Ryoma Ohi**[6], **Yihsuan S. Tsai**[1], **Aguirre A. de Cubas**[3], **Abid Khan**[1,7], **Ian J. Davis**[1], **Brian D. Strahl**[1,7], **Joel S. Parker**[1], **Ruhee Dere**[2], **Cheryl L. Walker**[2], and **W. K. Rathmell**[3]

[1]Lineberger Comprehensive Cancer Center, University of North Carolina, Chapel Hill, NC 27599

[2]Center for Precision Environmental Health, Department of Molecular and Cellular Biology, Baylor College of Medicine, Houston, TX 77030

[3]Vanderbilt-Ingram Cancer Center, Division of Hematology and Oncology, Department of Medicine, Vanderbilt University Medical Center, Nashville, TN 37232

[4]Department of Biology, New Mexico State University, Las Cruces, New Mexico 88003

[5]Texas A&M Health Sciences Center, Institute of Biosciences and Technology, Houston, TX

[6]Department of Cell and Molecular Biology, Vanderbilt University, Nashville, TN 37232

[7]Department of Biochemistry and Biophysics, University of North Carolina, Chapel Hill, NC 27599

Abstract

Loss of the short arm of chromosome 3 (3p) occurs early in >95% of clear cell renal cell carcinoma (ccRCC). Nearly ubiquitous 3p loss in ccRCC suggests haploinsufficiency for 3p tumor suppressors as early drivers of tumorigenesis. We previously reported methyltransferase *SETD2,* which trimethylates H3 histones on lysine 36 (H3K36me3) and is located in the 3p deletion, to also trimethylate microtubules on lysine 40 (αTubK40me3) during mitosis, with αTubK40me3 required for genomic stability. We now show that mono-allelic, *Setd2*-deficient cells retaining H3K36me3 but not αTubK40me3 exhibit a dramatic increase in mitotic defects and micronuclei count with increased viability compared to bi-allelic loss. In *SETD2*-inactivated human kidney cells, rescue with a pathogenic *SETD2* mutant deficient for microtubule (αTubK40me3) but not histone (H3K36me3) methylation replicated this phenotype. Genomic instability (micronuclei) was also a hallmark of patient-derived cells from ccRCC. These data show the *SETD2* tumor suppressor displays a haploinsufficiency phenotype disproportionately impacting microtubule methylation and serves as an early driver of genomic instability.

Address correspondence to: W. Kimryn Rathmell, MD, PhD, Division of Hematology and Oncology, 2220 Pierce Avenue, Preston Research Building, Suite 777, Vanderbilt-Ingram Cancer Center, Nashville, TN 37232, Phone: 615-875-9731, Fax: 615-343-7602, Kimryn.Rathmell@Vanderbilt.Edu.

Yun Chen Chiang, In Young Park, and Esteban A. Terzo contributed equally to this article

W. Kimryn Rathmell and Cheryl Lyn Walker contributed equally to this article

Disclosure of Potential Conflicts of Interest: No potential conflicts were disclosed.

Keywords

SETD2; genomic instability; micronuclei; renal cell carcinoma

Introduction

Many cancer types are characterized by large scale, characteristic alterations of chromosomal copy number. Clear cell renal cell carcinoma (ccRCC) is characterized by frequent inactivating mutations of the Von Hippel–Lindau (*VHL*) tumor suppressor gene (1), with accompanying loss of heterozygosity provided by a large deletion of chromosome 3p (2). Recent large-scale multiplatform sequencing techniques identified that, in addition to *VHL*, other tumor suppressor genes encoding epigenetic regulators such as *Polybromo 1 (PBRM1/BAF180)*, *BAP1*, and Set domain containing 2 (*SETD2*) are implicated in ccRCC tumorigenesis (3–5). Importantly, all of these commonly mutated genes reside in the same portion of affected chromosome 3p. Loss of 3p results in loss of heterozygosity (LOH) for all four of these genes, which individually acquire "second-hit" mutations and loss of function of the remaining allele in subsets of ccRCC. Of these, *SETD2* is of particular interest, as this tumor suppressor has been increasingly identified as a common mutation across cancer types, including lung (6), bladder (7), glioma (8) and leukemia (9).

SETD2 encodes a methyltransferase known to be the sole enzyme responsible for the trimethylation of lysine 36 on histone H3 (H3K36me3) (7, 8, 10–12). Bi-allelic deficiency of *SETD2* via deletions and inactivating mutations occur in up to 20% of primary human RCC tumors and it is associated with more advanced disease and the metastatic phenotype, typically lethal within 1–5 years (13). Bi-allelic loss of *SETD2* has been shown to result in loss of H3K36me3 in ccRCC-derived cells and tumors (9, 14, 15). Examination of H3K36me3 status in ccRCC cells of metastatic tumor specimens suggest that *SETD2* mutations may occur in over 50% of metastatic lesions (16). Furthermore, a study of ccRCC intratumoral heterogeneity identified distinct *SETD2* mutations across subsections of an individual tumor, suggesting a selection bias for *SETD2* mutation in the course of ccRCC development (7).

SETD2 is a multi-domain containing protein with distinct functions for each domain. The methyltransferase activity is mediated by a centrally-located SET domain. Mutations in this domain are common in ccRCC (10, 14), suggesting loss of catalytic activity is a critical event in tumor development. We previously characterized a pathogenic SET domain mutation found in ccRCC, an arginine-to-cysteine mutation at residue 1625 of SETD2 (R1625C) (15), which abolishes methylation activity. At its C-terminus, SETD2 also contains the Set2-Rpb1-interaction (SRI) domain (17). This domain mediates the interaction between SETD2 and the phosphorylated C-terminal domain of RNA polymerase II (RNAPII). We also identified a recurrent mutation in the SRI domain, an arginine-to-histidine mutation at residue 2510 (R2510H) (15). This mutation preserves the H3 trimethylation catalytic activity of SETD2, suggesting SETD2 may have other key functions in addition to its to the well-characterized role as a histone methyltransferase.

We recently discovered that SETD2 also functions as a microtubule methyltransferase, in addition to the well-characterized role of SETD2 in histone methylation (18). SETD2 trimethylates α-tubulin on lysine 40 (αTubK40me3) of microtubules and loss of this mark results in genomic instability. *SETD2*-null cells exhibit mitotic spindle and cytokinesis defects, polyploidy, and formation of micronuclei. Importantly, pathogenic *SETD2* mutations in the SET domain as well as the SRI domain were unable to methylate microtubules, and caused an increase in chromosome bridges and lagging chromosomes relative to wild-type SETD2, indicating that in addition to the catalytic domain, a functional SRI domain was also required for αTubK40me3 (18).

These mitotic alterations caused by loss of αTubK40me3 can lead to chromosomal abnormalities and genomic instability, hallmarks of tumorigenesis, and are thought to be an important source of genetic diversity and development of cell clones during tumor progression (19). In the case of the type of defects observed with *SETD2* mutants deficient in microtubule methylation (lagging and bridging chromosomes), this genomic instability results in the formation of micronuclei. Micronuclei contain acentric chromosome fragments, acentric chromatid fragments, or whole chromosomes that failed to migrate during mitosis, which are enclosed by nuclear membrane (20). The presence of micronuclei is a reliable cytological indicator of chromosome instability (21), and micronuclei are a common feature of many solid tumors and pre-neoplastic lesions (19,20), but have not been studied in any detail in ccRCC to date.

Here, we report that SETD2's ability to trimethylate microtubules and preserve genomic stability is dose dependent, and *SETD2* haploinsufficiency or reduced dosage, is sufficient to impair genomic stability and induce micronuclei formation. Using micronuclei as a readout of genomic instability in wild-type (WT) *SETD2* and *SETD2* disrupted human kidney proximal tubule epithelial cells (HKC), we confirmed that *SETD2* loss causes a significant increase in micronuclei. To directly demonstrate that *SETD2* haploinsufficiency was sufficient to induce genomic instability (micronuclei), we induced loss of a single copy of *Setd2* using $Setd2^{w/f}$ mouse embryonic fibroblasts (MEFs). Mono-allelic loss of *Setd2* was sufficient to increase lagging and bridging chromosomes, and caused a significant increase in micronuclei formation. Importantly, while promoting micronuclei accumulation, mono-allelic *SETD2* loss had no measurable effect on H3K36me3, but did cause loss of αTubK40me3, revealing a previously unrecognized effect of *SETD2* dosage. Comparing different *SETD2* mutations, we also found that the SRI-domain mutation, which rescues H3K36me3, but not αTubK40me3, fails to rescue micronuclei formation and mitotic defects in *SETD2*-deleted cells compared to WT *SETD2*. Importantly, micronuclei were also a common feature of 3p deleted ccRCC cell lines and were seen in a significant fraction of tumor cells from all patients with ccRCC. These data indicate that *SETD2* is haploinsufficient for αTubK40 trimethylating activity, with loss of microtubule methylation driving early genomic instability in tumors with 3p loss, preceding the loss of histone H3K36 trimethylation, and contributing to the progression of ccRCC. Moreover, our results shed light on a new mechanism by which mono-allelic inactivation of *SETD2* or 3p loss can drive tumorigenesis in other cancers, and points to microtubule methylation as a key tumor suppressive activity of SETD2.

Materials and Methods

Cell Cultures

Human renal cell carcinoma ACHN, UMRC2, Caki-1, and A498 cells were acquired from the American Type Culture Collection (Manassas, VA). RCC4 cells were generously provided by Dr. William Kim (UNC, Chapel Hill, NC). The SV-40 transformed human renal tubule epithelial cell line (HKC) was obtained from Dr. Lorraine Racusen, Baltimore, MD. All cells undergo annual STR confirmation. Human cell lines were cultured in Dulbecco's Modified Eagle Medium (DMEM, Gibco/Life Technologies, Carlsbad, CA) supplemented with 10% FBS (Gemini Bio-Products, West Sacramento, CA), non-essential amino acids, L-glutamine, penicillin, and streptomycin. For Setd2$^{w/f}$ and Setd2$^{f/f}$ mouse embryonic fibroblasts, cells were maintained in phenol-red free media (DMEM, high glucose, HEPES, no phenol red) supplemented with Sodium Pyruvate and GlutaMAX (ThermoFisher Scientific), to prevent any spontaneous activation of the Cre recombinase by estrogenic compounds found in phenol red containing media. All cultures were maintained at 37°C in 5% CO_2. The identify of all human cell lines employed in the present study has been authenticated using the Short Tandem Repeat (STR) profiling test offered by ATCC as a service. All cell lines have been tested for Mycoplasma contamination using the PCR-based ATCC's Universal Mycoplasma Detection test (catalog number: 30-10102K).

Generation of *Setd2$^{w/f}$* and *Setd2$^{f/f}$* mouse embryonic fibroblasts (MEFs)

The detailed information for generating *Setd2$^{w/f}$* and *Setd2$^{f/f}$* MEFs was described in a previous publication (18). In brief, *Setd2$^{w/f}$* or *Setd2$^{f/f}$* MEFs were generated from 13.5 days postcoitum (d.p.c.) embryos of *Setd2$^{w/f}$* or *Setd2$^{f/f}$* mice, respectively. The cells were spontaneously immortalized via serial passaging. The immortalized cells were transfected with an ER-Cre vector expressing Cre recombinase fused with a mutated ligand-binding domain for the human estrogen receptor (ER-Cre). Stable cell lines expressing ER-Cre were generated by selection using 5μg/ml blasticidin (Thermo Fisher Scientific).

Setd2$^{w/f}$ or *Setd2$^{f/f}$* MEFs expressing ER-Cre were treated with 3μM 4-hydroxytamoxifen (4-HT, the active metabolite of tamoxifen, Sigma-Aldrich) or vehicle (0.01% ethanol) for two days (or as indicated) for efficient *Setd2* knockout. The phenotype of *Setd2$^{w/f}$* MEFs is similar to that observed with bi-allelic loss (*Setd2$^{f/f}$*) (18), for which micronuclei were counted after two days of tamoxifen treatment, while the *Setd2$^{w/f}$* MEFs remain viable as a culture for several passages.

Generation of *SETD2*-null or mutation human kidney epithelial cells

To establish HKC *SETD2* null cells, HKC cells were transfected as previously described (15) with a pair transcription activator-like effector nucleases (TALENs) constructs targeting exon 3 (5′-TCATGTAACATCCAGGCC-3′ and 5′-ACAGCAGTAGCATCTCCA-3′) using Amaxa cell Line Nucleofector Kit V (Lonza, Basel, Switzerland) and single cell sorted to isolate single clones. Individual clones were screened for loss of H3K36me3 and sequenced at the *SETD2* target site to confirm the presence of inactivating mutations. The allelic sequencing confirmed the *SETD2* inactivation through frameshift mutations at the TALEN target site in both *SETD2* alleles.

Generation of SETD2 knockdown human kidney epithelial cells

HKC cells were infected with shRNA virus expressing either a Scramble (SCR) or shRNA against SETD2 (TRCN0000237839, Sigma). shSETD2 sequence obtained from the Broad Institute shRNA Library. Cells were passaged 24 hours post infection in media containing puromycin (1ug/ml). Following drug selection, cells were passaged once more at day 3 post shRNA virus infection. Subsequently, cells were fixed with either paraformaldehyde or methanol for immunostaining at 6 days post infection.

SNP array and 3p structural variation analysis

Genomic DNA was isolated from confluent 10cm plates using the Qiagen DNeasy Blood & Tissue Kit (Qiagen 69504) per manufacturer's standard protocols. SNP array was conducted on the Infinium Core-24 kit BeadChip (Illumina) by UNC Mammalian Genotyping Core according to manufacturer's standard protocols. The SNP data was pre-processed with Genomestudio v2 (Illumina) and the R package, genoCNV was used to estimate the copy number states and genotype calls for all interested cell lines. The allele-specific copy number analysis of tumors (ASCAT) algorithm (22) (version 2.5) was employed to calculate somatic whole-genome allele-specific copy number profiles (ASCAT-profiles), as well as estimates of cell ploidy.

Western Blot

Cells were lysed by gentle pipetting several times and incubated on ice for 10 mins in a cell fractionation buffer (320 mM sucrose, 10mM Tris-HCl (pH8.0), 2mM magnesium acetate, 3 mM calcium chloride, 0.1 mM EDTA, 0.5% NP-40, fresh 1mM dithiothreitol, protease inhibitor cocktail, 1 mM PMSF, and 1 mM sodium orthovanadate). Cytoplasmic fractions were collected after centrifugation at 1,000 g for 5 min and were used for western blots using antibodies against α-TubK40me3 (18, 23) or α-tubulin (MA1-19162, Thermo Fisher Scientific, Waltham, MA). The nuclear proteins were extracted in cell lysis buffer (20 mM Tris-HCl (pH7.5), 150 mM NaCl, 1mM EDTA, 1 mM EGTA, 1% Triton X-100, and protease inhibitor cocktail) by sonication for 3 cycles of 30 secs on/off using Bioruptor 300 (Diagenode, Denville, NJ) and used for western blots using antibodies against SETD2 (HPA042451, Sigma-Aldrich, St. Louis, MO), H3K36me3 (61101, Active Motif, Carlsbad, CA) or histone H3 (ab1791, Abcam, Cambridge, MA). The samples were separated on a 4–15% SDS-PAGE gel and transferred onto a PVDF membrane. Membranes were blocked in 5% non-fat milk in TBST (50 mM Tris pH 7.5, 150 mM NaCl, and 0.1% Tween 20) for 1 hr and immunoblotted using primary antibodies for overnight and secondary goat anti-mouse IgG-HRP (sc-2005, Santa Cruz Biotechnology, Dallas, TX) or goat anti-rabbit IgG-HRP (sc-2004, Santa Cruz Biotechnology) for 2 hrs.

For SETD2 knockdown HKC cells, lysates were separated on a 4–15% SDS-PAGE gel and the proteins were subsequently transferred to a PVDF membrane. Membranes were blocked in 5% non-fat milk in TBST and incubated O/N with primary antibodies in milk. Anti-β-Tubulin (05-661, EMD Millipore) antibody was used as loading control.

Immunofluorescence staining for micronuclei

HKC cells were cultured on chamber slides (Corning) for 16–18 hours and fixed using a 4% para-formaldehyde for 15 minutes. After three washes with cold PBS for 5 minutes each, the samples were permeabilized using a 0.25% Triton X-100 in PBS for 10 minutes and followed by 10-minute incubation with 1% hydrogen peroxide. After blocking in 5% BSA, cells were incubated at 4°C overnight with mouse anti LAP2 (1:500, Abcam) or human anti-CREST (1:6000, Antibody Inc) primary antibody. After four rounds of vigorous washing for 10 minutes each using PBST, cells were incubated for 1 hour at room temperature with goat anti-mouse IgG Alexa488 (Life technologies, 1:1000) and goat anti-human IgG H+L 568 (Life technologies, 1:1000) secondary antibody. After washing, cells were counterstained using DAPI for subsequent visualization of nuclei. Coverslips were mounted into chamber slides with ProLong Gold Antifade Mountant (Life technologies). Fluorescence signals were visualized using confocal microscopy (LSM 880, Zeiss). The number of micronuclei per 300 cells was counted and repeated for two times per coverslip. Data from three different coverslips in three independent experiments were manually quantitated.

For shRNA SETD2 knockdown of HKC cells, samples were fixed with cold methanol for 5 min at −20C, followed by three 5 min washes in PBS. Cells were then blocked in 2.5% BSA, 1% normal goat serum (NGS) in PBS for 1 hr followed by incubation with anti-LaminB1 (ab16048, Abcam) (1:250) antibody in PBS-BSA-NGS for 1 hr at RT. Cells were washed with PBS-0.1% Tween 20-NGS (PBST-NGS), followed by secondary antibody incubation for 30 min at RTπ. Cells were counterstained using DAPI (1:1000) for 5 min and then mounted on slides using Prolong Gold Antifade mounting media. Images were acquired on a Zeiss 800 Upright confocal microscope using a 63x/1.4 NA under default filter settings and pinhole of 1 airy unit. For every image, approximately ten Z-sections were acquired with an average of 0.4um thickness per slice. Z-stacks were processed in FIJI (Version 2.0.0) and images presented are maximum intensity projections of Z-stacks. The number of micronuclei per 150 cells per sample (shScramble and shSETD2) was counted and data from three independent experiments were manually quantitated.

Setd2 knockout was induced in MEFs (as described above), then fixed in 3.7% formaldehyde solution for 15 minutes, permeabilized in Triton-X 100 for 20 minutes and incubated for an hour in blocking buffer containing 3% bovine serum albumin (BSA) in 1XPBS at room temperature (RT). MEFs were then probed with human anti-CREST antibody (Antibody Inc) and anti-rabbit CENPB (Abcam, ab25734) for an hour at RT. Alexafluor 568- and 488-conjugated secondary antibodies (Invitrogen) were used to detect anti-CREST and anti-CENPB respectively while DNA was stained using Hoechst 33342 (Invitrogen). Immunoflourescence images were taken using Zeiss Axiovert 200M-inverted Microscope equipped with epifluorescence optics and an Apotome structured illumination module (Carl Zeiss) or a 60X 1.4 NA objective (Olympus) on a DeltaVision Elite imaging system (GE Healthcare) equipped with a Cool SnapHQ2 CCD camera (Roper), and processed using ratio deconvolution in SoftWorx (GE Healthcare). Total CREST (+) micronuclei were counted per 100 micronuclei per coverslip from three independent experiments.

Immunofluorescence staining for mitotic defects

Cells were cultured on cover slips and fixed using ice cold Methanol for 10 minutes and followed by permeabilization using a 0.2% Triton X-100 solution in PBS buffer for 5 minutes. After three washes using PBS buffer, the cells were blocked in 2% BSA blocking buffer for 30 minutes at RT. Cells were incubated in blocking buffer using primary antibodies overnight at 4°C. Primary antibodies were diluted as follows; rabbit anti-H3K36me3 (1:1000, Abcam), mouse anti-α-tubulin (1:400, clone DMIA, Sigma) and human anti-centromere (1:6000, Antibody Inc). After five rounds of vigorous washing for 10 minutes each using PBST, cells were incubated for 1 hour in blocking buffer with corresponding secondary antibodies (donkey anti-rabbit (clone 488, Life technologies), goat anti-mouse IgG H&L Cy5 (Abcam) and goat anti-human IgG H+L (clone 568, Life technologies) at a dilution of 1:1000. Following more than three washes, for 10 minutes each using PBST, cells were counterstained using DAPI for subsequent visualization of nuclei. Coverslips were mounted in ProLong Gold Antifade Mountant (Life technologies) and cells visualized using confocal microscopy (LSM 880, Zeiss).

Immunofluorescence staining for micronuclei in human ccRCC

Human primary RCCs were obtained under an approved IRB protocol with patients providing written informed consent to de-identified use of tissue. The studies were conducted in accordance with recognized ethical guidelines (e.g., Belmont Report).

Approval was granted by the Vanderbilt Biomedical IRB. Following pathological assessment, extra tissue is freshly provided, cells were dispersed by mechanical dissociation, followed by enzymatic digestion using collagenase and DNase. Single cell suspension was passed over 70μm strainer then subjected to red blood cell lysis. Samples were then mounted with Wescor Cytopro cytocentrifuge and fixed with 4% PFA (Electron Microscopy Sciences) in Cytoskeleton Buffer (10mM MES pH6.1, 138mM KCl, 3mM $MgCl_2$, 2 mM EGTA, 320mM sucrose) for 10 minutes. Cells were permeabilized with 0.1% TritonX-100 in PBS (PBSTx), blocked with 1% BSA in PBSTx, stained for pan-cytokeratin (AE1/AE3+5D3, Abcam ab86734, 1:100 in 1% BSA in PBSTx) and DAPI, then mounted with Prolong Gold Antifade reagent (Thermo Fisher Scientific). For secondary antibody staining, Alexa Fluor® 488 AffiniPure Donkey Anti-Mouse IgG (Jackson ImmunoResearch, 715-545-151, 1:500) was used. Images were acquired on a Zeiss LSM880 or LSM710 confocal microscopes using 63x/1.40 Plan-Apochromat oil objective and 405nm and 488nm lasers, default filter settings and pinhole of 1 airy unit or Deltavision Elite Imaging System. Images were processed in FIJI (Version 2.0.0) and images presented are maximum intensity projections of individual cells.

Immunohistochemistry

For H3K36me3 immunohistochemistry (IHC), patient de-identified, formalin fixed and paraffin (FFPE) embedded ccRCC samples were sectioned and hematoxylin and eosin (H&E) stained by Vanderbilt University Medical Center Translational Pathology Shared Resource. To perform H3K36me3 immunohistochemistry, FFPE sections were deparaffinized, then incubated for 45 minutes in heated citric acid buffer (10mM citric acid, 0.05% Tween-20, pH 6.o) for antigen retrieval. Slides were then stained with H3K36me3

antibody (Abcam, ab9050, 1:500), using the Cell and Tissue Staining Kit (Rabbit, HRP-DAB System, R&D Systems), according to manufacturer's protocol.

Reverse transcriptase–PCR

The total RNAs were isolated from *Setd2*$^{w/w}$, *Setd2*$^{f/w}$, and *Setd2*$^{f/f}$ MEFs treated with 4-hydroxytamoxifen for 0, 3, and 6 days using RNeasy mini kit (Qiagen), and their complementary DNAs were synthesized using Supersciprt III reverse transcriptase (Invitrogen). The quantities of *Setd2* mRNAs were assessed by real-time quantitative PCR using specific TaqMan probes (ThermoFisher, Mm01250234_m1) amplifying exon 6, which is the region to be deleted by Cre recombination, and a TaqMan Fast Universal master mix on QuantStudio Flex Real-Time PCR system (ThermoFisher). The quantities of *Setd2* mRNAs were normalized to those of glyceraldehyde 3-phosphate dehydrogenase, which was used as an endogenous control. The following set of conditions were used for each real-time reaction: 95°C for 20 minutes followed by 40 cycles of 1 second at 95°C and 20 seconds at 60°C. The real-time PCR reactions were performed in triplicate twice and quantified using the −ΔΔ cycle threshold (CT) method.

Statistics

Densitometry analyses using ImageStudio Ver2.0 were performed on immunoblots of H3K36me3 and αTubK40me3 normalized to H3 and αTubulin, respectively. Significance was inferred with Tukey's multiple comparison test. To determine significance of micronuclei count or percentage and of mitotic defects from triplicates, we performed a two-way ANOVA test, which shows significant interactions between samples. We performed Student's t-Test using a paired, two-tailed distribution to determine significance of qRT-PCR and micronuclei count in SETD2 knockdown HKC data sets. A reported *p*-value of less than 0.05 is considered significant. All analyses were performed using Prism 7 (GraphPad) and Excel (Microsoft) software.

Results

SETD2 loss is sufficient to induce genomic instability in normal human kidney proximal tubule epithelial cells

Previous studies have linked *SETD2* inactivation to genomic instability in RCC utilizing tumor-derived analysis (24). We first asked if loss of this tumor suppressor alone was sufficient to promote genomic instability in non-tumor kidney epithelial cells. To answer this question, and to examine the domain(s) of SETD2 required for maintenance of genomic stability in normal kidney epithelial cells, we utilized a cell line generated from immortalized normal human kidney proximal epithelial cells (HKC), which retain a normal chromosome 3 (Supplementary Fig. S1A). *SETD2* was inactivated in the parental HKC line (*SETD2* −/−), and a series of rescue lines generated by re-expressing SETD2. This panel included lines rescued with a fully functional wild-type N-terminal truncated SETD2 (tSETD2), a tSETD2 catalytically-dead SET domain-mutant (R1625C), and a tSETD2 SRI domain-mutant (R2510H). Genomic instability was a prominent feature of *SETD2* −/− HKC cells expressing empty vector (GFP), catalytically-dead SET domain mutant tSETD2 R1625C, or the SRI domain mutant tSETD2 R2510H (Fig. 1A). SETD2-deficient cells

exhibited a significant increase in both lagging chromosomes and chromosome bridge defects (Fig. 1A–C). Thus, as previously seen in RCC-derived 786-0 cells (18), in normal kidney epithelial cells both the SET and SRI domains were required to maintain genomic stability: an increased incidence of mitotic defects occurred when SETD2 activity is absent or when it carries pathogenic mutations in either of these two functional domains.

This genotype-phenotype correlation was extended using micronuclei as a readout of genomic instability. Micronuclei were evident as punctate, DAPI-positive structures that were also immunoreactive with CREST (anti-centromere) antibody. Only wild-type SETD2 (tSETD2) could rescue genomic instability in *SETD2* −/− HKC cells and reduce micronuclei count to normal levels (Fig. 2A). Neither empty vector (GFP), catalytically-dead SET domain R1625C, nor SRI domain R2510H SETD2 mutants rescued the increase in micronuclei observed in *SETD2* −/− HKC. Further, *SETD2* −/− HKC cells showed both CREST (+) and CREST (−) micronuclei, indicative of entire or fragmented chromosomes (Fig. 2B and C). This was also the case in *SETD2* −/− HKC cells reconstituted with catalytically-dead SET domain (R1625C) and SRI domain (R2510H) *tSETD2* mutants (Fig. 2B and C).

Micronuclei were also a common feature of a panel of ccRCC-derived cell lines, relative to ACHN cells, a known wild-type *VHL* line cytogenetically similar to papillary type renal cell carcinomas (25). Single nucleotide polymorphism (SNP) arrays using Log2R and B allele frequency score confirmed that all of the ccRCC-derived cells displayed chromosome 3p deletion. However, ACHN and proximal tubule kidney epithelial HKC cells (26) retained two normal copies of chromosome 3, and had a lower micronuclei count relative to the other ccRCC-derived cells (Supplementary Fig. S1A–D).

One question that arises is whether the cells that have experienced genomic instability as a result of SETD2 depletion remain in the population and perpetuate these genomic changes as potential clonal features furthering the process of tumorigenesis. As an indicator of this process, we tested the copy number variation (CNV) of both *SETD2* proficient (+/+) and *SETD2* deficient (−/−) HKC cells. ASCAT-profiles of both HKC cell lines harboring empty GFP-containing vector revealed an increase of genomic instability upon *SETD2* loss characterized by gains and losses of parts of, or entire, chromosomes, supporting the notion that changes in SETD2 activity contribute to the genomic instability of tumor cells (Supplementary Fig. S2A and B).

Mono-allelic loss of SETD2 is sufficient to abrogate microtubule methylation and increase micronuclei formation

In cells lacking SETD2, both microtubule and histone methylation are abrogated (18). To determine the impact of reduced *SETD2* dosage (mono-allelic loss) on microtubule vs. histone methylation, we employed tamoxifen-inducible ER-Cre wild-type *Setd2* (w/w), heterozygous (w/f) and homozygous (f/f) *Setd2* mutant mouse embryonic fibroblasts (MEFs). These cells lack the genetic diversity found in cancer cell lines, thus allowing for *Setd2* alterations to be examined in isolation from other genetic aberrations, and for drawing causal associations between mono- and bi-allelic *Setd2* loss and genomic stability.

We first compared the effects of mono- and bi-allelic *Setd2* loss on histone (H3K36me3) and microtubule (αTubK40me3) methylation. Strikingly, while *Setd2*$^{w/f}$ MEFs exhibited reduction of αTubK40me3, observed in multiple clones whose relative Setd2 mRNA levels were shown to be partially reduced compared to those of *Setd2*$^{w/w}$ MEFs (Supplementary Fig. S3A and B), mono-allelic loss of *Setd2* caused no change in H3K36me3 levels (Fig. 3A). Conversely, *Setd2*$^{f/f}$ MEFs showed a complete loss of both microtubule and histone methylation, consistent with complete loss of SETD2 methyltransferase activity (Fig. 3A). Thus, mono-allelic *SETD2* was haploinsufficient for microtubule, but not chromatin, methylation.

To explore the effect of *SETD2* mono-allelic loss on genomic stability, we quantitated acute chromosomal defects in *Setd2*$^{w/w}$ and *Setd2*$^{w/f}$ MEFs following excision of *Setd2*. Relative to *Setd2*$^{w/w}$ MEFs, *Setd2*$^{w/f}$ MEFs exhibited evidence for chromosome lagging and bridging, the same mitotic defects seen in *SETD2*-deficient HKC cells, and a significant increase in micronuclei (Fig. 3B–D). These data demonstrate that when *Setd2* gene dosage is reduced by mono-allelic loss of *Setd2*, this deficit is sufficient to decrease αTubK40me3, and cause both mitotic chromosome defects and a statistically significant increase in micronuclei. The mitotic phenotype of these cells is similar to that observed with bi-allelic loss (18).

As noted above, micronuclei can contain whole chromosomes or acentric chromosome fragments, both of which can occur as a result of mitotic defects (lagging and bridging chromosomes). Micronuclei of *Setd2*$^{f/f}$ and *Setd2*$^{w/f}$ MEFs stained with Hoechst, CENPB and CREST also exhibited both CREST (+) whole chromosome and CREST (−) acentric chromosome staining (Fig. 4A). Both *Setd2*$^{f/f}$ and *Setd2*$^{w/f}$ MEFs showed increased total micronuclei number, but homozygous *Setd2* MEFs (*Setd2*$^{f/f}$) showed a more dramatic increase in Hoechst (+) CENPB/CREST (−) micronuclei, containing acentric chromosome fragments, compared to *Setd2*$^{w/f}$ MEFs (Fig. 4B and Supplementary Fig. S4A). Remarkably, MEFs with mono-allelic loss of *Setd2* (*Setd2*$^{w/f}$) showed the most dramatic increase in Hoechst/CENPB/CREST (+) micronuclei, suggesting these micronuclei arose predominantly from segregation defects involving whole chromosomes (Fig. 4B and Supplementary Fig. S4A and B). Importantly, given that MEFs with mono-allelic loss of *Setd2* (*Setd2*$^{w/f}$) were proficient for H3K36me3 histone methylation, these data suggest that genomic instability associated with haploinsufficiency is independent of the histone methyltransferase activity of SETD2. In agreement with the latter results, partial *SETD2* knockdown (~30% decrease) using shRNA on *SETD2*-proficient HKC cells further demonstrates that reduced SETD2 levels significantly increase micronuclei count (Supplementary Fig. S5A–D). Further, as noticed with *Setd2*$^{w/f}$ MEFs, the same partial *SETD2* knockdown was sufficient to promote mitotic defects in HKC cells (Supplementary Fig. S5E).

Genomic instability is a feature of ccRCC patient-derived tumors

To link the causal associations seen *in vitro* between mono-allelic loss of *SETD2* and genomic instability, we utilized tumor cells derived from ccRCC patients to determine if the nearly ubiquitous and early loss of chromosome 3p seen in these tumors resulted in loss of

genomic stability. Using micronuclei as an indicator for loss of genomic stability, tumor-derived and adjacent normal kidney cells from five ccRCC patients were stained with DAPI (DNA) to quantitate micronuclei, and pan-cytokeratin as a marker for normal epithelial and ccRCC cells (Fig. 5). Remarkably, tumor cells from all five ccRCC patient-derived samples exhibited a significantly increased frequency of micronuclei (Table 1). The frequency of micronuclei in tumor cells ranged from 1.1% to 30%. Micronuclei were detected in only one matched normal sample, but in that individual, the frequency of micronuclei was 2-fold higher in tumor vs. matched normal cells. The histology of these tumors was confirmed to be clear cell, and nuclei of these tumors stained positive for histone methylation (Supplementary Fig. S6A), confirming that these tumors retained H3K36 trimethylating activity. Additionally, sequencing available tissue from the ccRCC tumor samples identified none with deleterious *SETD2* mutations (Supplementary Fig. S6B).

To explore if increase in micronuclei count is observed in other types of kidney cancer characterized by retaining chromosome 3p, we DAPI stained tumor-derived and adjacent normal kidney cells from two papillary RCCs (pRCCs) and two oncocytoma patients and quantitated micronuclei. In these patient-derived samples, we found lower micronuclei counts compared to those in ccRCC-derived tumor cells (Table 1).

Thus, ccRCC cell lines and ccRCC patient-derived tumor cells exhibit both the genomic instability (micronuclei) associated with mono-allelic *SETD2* deletion, as a consequence of chromosome 3p loss, as well as the dependence on the SRI domain for nonhistone methylating SETD2 function. Together, these data demonstrate that micronuclei formation occurs with mono-allelic loss of *SETD2 in vivo*, in line with our *in vitro* observations, pointing to genomic instability and micronuclei as early and common features caused by the 3p loss in ccRCC.

Discussion

The vast majority (in excess of 95%) of ccRCCs have *SETD2* haploinsufficiency as a consequence of chromosome 3p loss, and this chromosomal event is widely accepted to be an early event in ccRCC transformation (27). Based on our previous and current data, we postulate that *SETD2* haploinsufficiency plays a crucial role as a driver during early ccRCC disease development. In addition, an independent report, using high-resolution profiling of H3K36me3 in metastatic ccRCC tumor samples, suggests that decreased *SETD2* mRNA expression, after mono-allelic loss, is not sufficient to alter SETD2's histone H3 lysine methyltransferase activity (16). Our findings consistently demonstrate SETD2 acting as a dual-function methyltransferase, here identifying a scenario in which staged loss of function separates these activities. Heterozygosity for *SETD2* provides an opportunity for genomic instability to promote early disease development, potentially creating conditions permissive to the harsher setting of bi-allelic loss, and complete loss of trimethylation functionality. Based on these and other data, we propose a stepwise model for loss of SETD2 functionality as a driver in ccRCC. First, with the loss of 3p and haploinsufficiency for SETD2 as an early event contributing to genomic instability, and upon bi-allelic inactivation, the additional loss of H3K36 trimethylating activity (Fig. 6).

SETD2 is mutated or lost in a growing list of tumors (6–9), and notably mutations in *SETD2* are enriched in chemotherapy refractory pediatric acute lymphocytic leukemia (9, 28). The frequency with which these mutations occur in one allele without loss of heterozygosity has not been examined in detail. Further, 3p is a commonly deleted genomic region, raising the possibility that haploinsufficiency for SETD2 function may be a more common event in tumorigenesis than previously considered. It is important to consider, however, that in ccRCC tumors (that routinely lose 3p), haploinsufficiency for a number of important proteins may be playing a role in permitting tumorigenesis. Indeed, preliminary studies have implicated BAP1, another 3p localized gene, as a potential mediator in the haploinsufficient state (29). Future studies will need to consider the effect of multigene haploinsufficiency in promoting tumorigenesis.

Beyond loss of genomic stability, bi-allelic *SETD2* inactivation may contribute to tumorigenesis in several ways, in particularly in mediating DNA repair (30). SETD2's expanding function as a methylating enzyme has revealed that, in addition to the H3K36me3 mark on histones, SETD2 trimethylates lysine 40 on α-tubulin of mitotic microtubules (18) and the transcription factor STAT1 (31). In the case of SETD2's microtubule methylating function, failure to trimethylate αTubK40, in the setting of acute *Setd2* loss, is accompanied by loss of the αTubK40me3 mark from mitotic microtubules, and catastrophic mitotic defects (18). These acute effects we previously observed following *SETD2* loss were unlikely to be accounted for by loss of histone methylation, as conversion of histone methylation is considered to be a slow process over several cell divisions, and RNA-seq revealed no consistent alterations in gene expression associated with acute *SETD2* loss (18). Here, we report that mono-allelic *SETD2* loss is sufficient to cause genomic instability (lagging and bridging chromosomes and micronuclei), which is linked to SRI domain defects that uncouple SETD2's histone methylating from its newly discovered tubulin methylating activity. Other targets of SETD2 methylation are emerging, notably STAT1 (31), for which the impact of SETD2 haploinsufficiency is unknown. Further, genomic instability in human ccRCC tumors that were haploinsufficient for *SETD2*, but which retained H3K36 trimethylation, further supports the linkage between microtubule methylation by SETD2 and genomic stability. These data also point to micronuclei formation as a cytological tool to reveal novel aspects of *SETD2* function as a multifunctional tumor suppressor critical to genome maintenance.

Micronuclei were identified and described in erythrocytes first by W. Howell (1890) and later on by J. Jolly (1905) (32) as small, extranuclear chromatin bodies surrounded by a nuclear envelope which originate from acentric chromosome fragments or entire chromosomes lagging behind the main chromatin mass during anaphase (33, 34). Today, it is accepted that micronuclei represent a faithful cellular indicator of chromosome instability (or genomic instability), as high micronuclei frequency is associated with chromosome instability observed in many solid tumors and pre-neoplastic lesions (35, 36). Importantly, micronuclei have also been documented in primary cancers (33, 35), although ccRCC has not been well characterized in this regard. We show that micronuclei are a common feature not only among ccRCC-derived cell lines, but more importantly among ccRCC patient-derived tumors. Considering the typical low mitotic rate of primary RCC tumors, the

accumulations of micronuclei at the rates we observed implicate chromosome instability as a major driver of ccRCC tumorigenesis.

In showing that *SETD2* haploinsufficiency, and partially reduced levels of SETD2, are sufficient to initiate a wide range of mitotic defects resulting in lagging chromosomes and micronuclei formation, our data further underscore a much more complex role for SETD2 in genome maintenance than previously appreciated. While some of the more dramatic examples may represent mitotic failures, the persistence of micronuclei implies that some aberrant mitoses are permitted, possibly as a result of a failed checkpoint. In cells lacking *SETD2*, we were able to show evidence of an unstable genome, although this model does not fully address the haploinsufficient state. The bypassed checkpoint allowing these cells to persist remains an object of future investigation. In this regard, the shared genomic instability phenotype seen with *SETD2* haploinsufficiency and SRI-domain defects that abrogate microtubule but not histone methylation argues that maintenance of genomic stability by SETD2 is linked to its function as a microtubule methyltransferase. These data also suggest αTubK40 trimethylation is more sensitive to SETD2 stoichiometry fluctuations than H3K36 trimethylation. The effect of *SETD2* haploinsufficiency on any other targets is not known. These data strongly support the notion of αTubK40me3 playing a specialized role in maintaining genomic stability during mitosis. Dissecting the tubulin dynamics that govern this process, and the specialized role of SETD2 and the SRI domain in regulating αTubK40 methylation will be an important future goal.

It is now well accepted that the main drivers of cancer are not limited to highly penetrant dominant and recessive mutations, but also include heterozygous losses giving rise to haploinsufficiency states (37). There is an ever-increasing number of tumor suppressor genes known to display haploinsufficiency, such as PTEN and p53 (among others), with some pathways showing a higher tendency to dosage sensitivity than others (37–39). Another example of haploinsufficiency in cancer progression is PERK, an endoplasmic reticulum transmembrane protein kinase, displaying pro-tumorigenic activity in melanomas harboring activated $Braf^{V600E}$ mutation. However, deletion of one allele of PERK is permissive for $Braf^{V600E}$–dependent transformation, while excision of both alleles did not cooperate with $Braf^{V600E}$ in melanoma tumorigenicity (40). Interestingly, PERK mutations decreasing its activity are seen at a 7% frequency (40). Therefore, our compelling results showing SETD2 dose-dependent methyltransferase activity are in line with the work previously done in other cancer types, and demonstrate a crucial, and previously unappreciated, role of *SETD2* haploinsufficiency caused by 3p loss in progression of ccRCC.

Supplementary Material

Refer to Web version on PubMed Central for supplementary material.

Acknowledgments

Grant Support

The authors acknowledge support from the NIH: R01GM086610 (R. Ohi), R01CA203012 (W.K. Rathmell and C.L. Walker), R01CA198482 (W.K. Rathmell, I.J. Davis, B. D. Strahl), T32CA119925 (E.A. Terzo), T32CA009156 (Y.C. Chiang). R. Ohi acknowledges support from the Leukemia and Lymphoma Society.

We used the Zeiss LSM880 Airyscan and LSM 710 microscopes (NIH S10; 1S10OD021630-01) at the Vanderbilt University Cell Imaging Shared Resource (CISR) facility, the Integrated Microscopy Core at Baylor College of Medicine (NIH DK56338, and CA125123), CPRIT (RP15078), the Dan L. Duncan Comprehensive Cancer Center, and the John S. Dunn Gulf Coast Consortium for Chemical Genomics. We used the Flow Cytometry Core Facility at UNC supported in part by the Cancer Center Core Support Grant (P30 CA16086) to the UNC Lineberger Comprehensive Cancer Center.

References

1. Kaelin WG Jr. The von Hippel-Lindau tumor suppressor gene and kidney cancer. Clin Cancer Res. 2004; 10(18 Pt 2):6290S–5S. [PubMed: 15448019]
2. Kovacs G, Szucs S, De Riese W, Baumgartel H. Specific chromosome aberration in human renal cell carcinoma. Int J Cancer. 1987; 40(2):171–8. [PubMed: 3610386]
3. Dalgliesh GL, Furge K, Greenman C, Chen L, Bignell G, Butler A, et al. Systematic sequencing of renal carcinoma reveals inactivation of histone modifying genes. Nature. 2010; 463(7279):360–3. [PubMed: 20054297]
4. Pena-Llopis S, Vega-Rubin-de-Celis S, Liao A, Leng N, Pavia-Jimenez A, Wang S, et al. BAP1 loss defines a new class of renal cell carcinoma. Nat Genet. 2012; 44(7):751–9. [PubMed: 22683710]
5. Varela I, Tarpey P, Raine K, Huang D, Ong CK, Stephens P, et al. Exome sequencing identifies frequent mutation of the SWI/SNF complex gene PBRM1 in renal carcinoma. Nature. 2011; 469(7331):539–42. [PubMed: 21248752]
6. Walter DM, Venancio OS, Buza EL, Tobias JW, Deshpande C, Gudiel AA, et al. Systematic In Vivo Inactivation of Chromatin-Regulating Enzymes Identifies Setd2 as a Potent Tumor Suppressor in Lung Adenocarcinoma. Cancer Res. 2017; 77(7):1719–29. [PubMed: 28202515]
7. Cerami E, Gao J, Dogrusoz U, Gross BE, Sumer SO, Aksoy BA, et al. The cBio cancer genomics portal: an open platform for exploring multidimensional cancer genomics data. Cancer Discov. 2012; 2(5):401–4. [PubMed: 22588877]
8. Fontebasso AM, Schwartzentruber J, Khuong-Quang DA, Liu XY, Sturm D, Korshunov A, et al. Mutations in SETD2 and genes affecting histone H3K36 methylation target hemispheric high-grade gliomas. Acta Neuropathol. 2013; 125(5):659–69. [PubMed: 23417712]
9. Zhu X, He F, Zeng H, Ling S, Chen A, Wang Y, et al. Identification of functional cooperative mutations of SETD2 in human acute leukemia. Nat Genet. 2014; 46(3):287–93. [PubMed: 24509477]
10. Li J, Duns G, Westers H, Sijmons R, van den Berg A, Kok K. SETD2: an epigenetic modifier with tumor suppressor functionality. Oncotarget. 2016; 7(31):50719–34. [PubMed: 27191891]
11. Parker H, Rose-Zerilli MJ, Larrayoz M, Clifford R, Edelmann J, Blakemore S, et al. Genomic disruption of the histone methyltransferase SETD2 in chronic lymphocytic leukaemia. Leukemia. 2016; 30(11):2179–86. [PubMed: 27282254]
12. Sun XJ, Wei J, Wu XY, Hu M, Wang L, Wang HH, et al. Identification and characterization of a novel human histone H3 lysine 36-specific methyltransferase. J Biol Chem. 2005; 280(42):35261–71. [PubMed: 16118227]
13. Ho TH, Kapur P, Joseph RW, Serie DJ, Eckel-Passow JE, Tong P, et al. Loss of histone H3 lysine 36 trimethylation is associated with an increased risk of renal cell carcinoma-specific death. Mod Pathol. 2016; 29(1):34–42. [PubMed: 26516698]
14. Simon JM, Hacker KE, Singh D, Brannon AR, Parker JS, Weiser M, et al. Variation in chromatin accessibility in human kidney cancer links H3K36 methyltransferase loss with widespread RNA processing defects. Genome Res. 2014; 24(2):241–50. [PubMed: 24158655]
15. Hacker KE, Fahey CC, Shinsky SA, Chiang YJ, DiFiore JV, Jha DK, et al. Structure/Function Analysis of Recurrent Mutations in SETD2 Protein Reveals a Critical and Conserved Role for a SET Domain Residue in Maintaining Protein Stability and Histone H3 Lys-36 Trimethylation. J Biol Chem. 2016; 291(40):21283–95. [PubMed: 27528607]
16. Ho TH, Park IY, Zhao H, Tong P, Champion MD, Yan H, et al. High-resolution profiling of histone h3 lysine 36 trimethylation in metastatic renal cell carcinoma. Oncogene. 2016; 35(12):1565–74. [PubMed: 26073078]

17. Kizer KO, Phatnani HP, Shibata Y, Hall H, Greenleaf AL, Strahl BD. A novel domain in Set2 mediates RNA polymerase II interaction and couples histone H3 K36 methylation with transcript elongation. Mol Cell Biol. 2005; 25(8):3305–16. [PubMed: 15798214]
18. Park IY, Powell RT, Tripathi DN, Dere R, Ho TH, Blasius TL, et al. Dual Chromatin and Cytoskeletal Remodeling by SETD2. Cell. 2016; 166(4):950–62. [PubMed: 27518565]
19. Holland AJ, Cleveland DW. Boveri revisited: chromosomal instability, aneuploidy and tumorigenesis. Nat Rev Mol Cell Biol. 2009; 10(7):478–87. [PubMed: 19546858]
20. Wang Y, Waters J, Leung ML, Unruh A, Roh W, Shi X, et al. Clonal evolution in breast cancer revealed by single nucleus genome sequencing. Nature. 2014; 512(7513):155–60. [PubMed: 25079324]
21. Navin N, Kendall J, Troge J, Andrews P, Rodgers L, McIndoo J, et al. Tumour evolution inferred by single-cell sequencing. Nature. 2011; 472(7341):90–4. [PubMed: 21399628]
22. Van Loo P, Nordgard SH, Lingjaerde OC, Russnes HG, Rye IH, Sun W, et al. Allele-specific copy number analysis of tumors. Proc Natl Acad Sci U S A. 2010; 107(39):16910–5. [PubMed: 20837533]
23. Park IY, Chowdhury P, Tripathi DN, Powell RT, Dere R, Terzo EA, et al. Methylated alpha-tubulin antibodies recognize a new microtubule modification on mitotic microtubules. MAbs. 2016; 8(8): 1590–7. [PubMed: 27594515]
24. Kanu N, Gronroos E, Martinez P, Burrell RA, Yi Goh X, Bartkova J, et al. SETD2 loss-of-function promotes renal cancer branched evolution through replication stress and impaired DNA repair. Oncogene. 2015; 34(46):5699–708. [PubMed: 25728682]
25. Kovacs G, Fuzesi L, Emanual A, Kung HF. Cytogenetics of papillary renal cell tumors. Genes Chromosomes Cancer. 1991; 3(4):249–55. [PubMed: 1958590]
26. Racusen LC, Monteil C, Sgrignoli A, Lucskay M, Marouillat S, Rhim JG, et al. Cell lines with extended in vitro growth potential from human renal proximal tubule: characterization, response to inducers, and comparison with established cell lines. J Lab Clin Med. 1997; 129(3):318–29. [PubMed: 9042817]
27. Cancer Genome Atlas Research N. Comprehensive molecular characterization of clear cell renal cell carcinoma. Nature. 2013; 499(7456):43–9. [PubMed: 23792563]
28. Mar BG, Bullinger LB, McLean KM, Grauman PV, Harris MH, Stevenson K, et al. Mutations in epigenetic regulators including SETD2 are gained during relapse in paediatric acute lymphoblastic leukaemia. Nat Commun. 2014; 5:3469. [PubMed: 24662245]
29. Togo Y, Yoshikawa Y, Suzuki T, Nakano Y, Kanematsu A, Zozumi M, et al. Genomic profiling of the genes on chromosome 3p in sporadic clear cell renal cell carcinoma. Int J Oncol. 2016; 48(4): 1571–80. [PubMed: 26891804]
30. Mar BG, Chu SH, Kahn JD, Krivtsov AV, Koche R, Castellano CA, et al. SETD2 alterations impair DNA damage recognition and lead to resistance to chemotherapy in leukemia. Blood. 2017; 130(24):2631–41. [PubMed: 29018079]
31. Chen K, Liu J, Liu S, Xia M, Zhang X, Han D, et al. Methyltransferase SETD2-Mediated Methylation of STAT1 Is Critical for Interferon Antiviral Activity. Cell. 2017; 170(3):492–506. e14. [PubMed: 28753426]
32. Fenech M, Kirsch-Volders M, Natarajan AT, Surralles J, Crott JW, Parry J, et al. Molecular mechanisms of micronucleus, nucleoplasmic bridge and nuclear bud formation in mammalian and human cells. Mutagenesis. 2011; 26(1):125–32. [PubMed: 21164193]
33. Hatch EM, Fischer AH, Deerinck TJ, Hetzer MW. Catastrophic nuclear envelope collapse in cancer cell micronuclei. Cell. 2013; 154(1):47–60. [PubMed: 23827674]
34. Hintzsche H, Hemmann U, Poth A, Utesch D, Lott J, Stopper H, et al. Fate of micronuclei and micronucleated cells. Mutat Res-Rev Mutat. 2017; 771:85–98.
35. Gisselsson D, Bjork J, Hoglund M, Mertens F, Dal Cin P, Akerman M, et al. Abnormal nuclear shape in solid tumors reflects mitotic instability. Am J Pathol. 2001; 158(1):199–206. [PubMed: 11141493]
36. Terradas M, Martin M, Genesca A. Impaired nuclear functions in micronuclei results in genome instability and chromothripsis. Arch Toxicol. 2016; 90(11):2657–67. [PubMed: 27542123]

37. Berger AH, Pandolfi PP. Haplo-insufficiency: a driving force in cancer. J Pathol. 2011; 223(2):137–46. [PubMed: 21125671]

38. Bardeesy N, Sinha M, Hezel AF, Signoretti S, Hathaway NA, Sharpless NE, et al. Loss of the Lkb1 tumour suppressor provokes intestinal polyposis but resistance to transformation. Nature. 2002; 419(6903):162–7. [PubMed: 12226664]

39. Miyoshi H, Nakau M, Ishikawa TO, Seldin MF, Oshima M, Taketo MM. Gastrointestinal hamartomatous polyposis in Lkb1 heterozygous knockout mice. Cancer Res. 2002; 62(8):2261–6. [PubMed: 11956081]

40. Pytel D, Gao Y, Mackiewicz K, Katlinskaya YV, Staschke KA, Paredes MC, et al. PERK Is a Haploinsufficient Tumor Suppressor: Gene Dose Determines Tumor-Suppressive Versus Tumor Promoting Properties of PERK in Melanoma. PLoS Genet. 2016; 12(12):e1006518. [PubMed: 27977682]

Significance

Loss of a single allele of a chromatin modifier plays a role in promoting oncogenesis, underscoring the growing relevance of tumor suppressor haploinsufficiency in tumorigenesis.

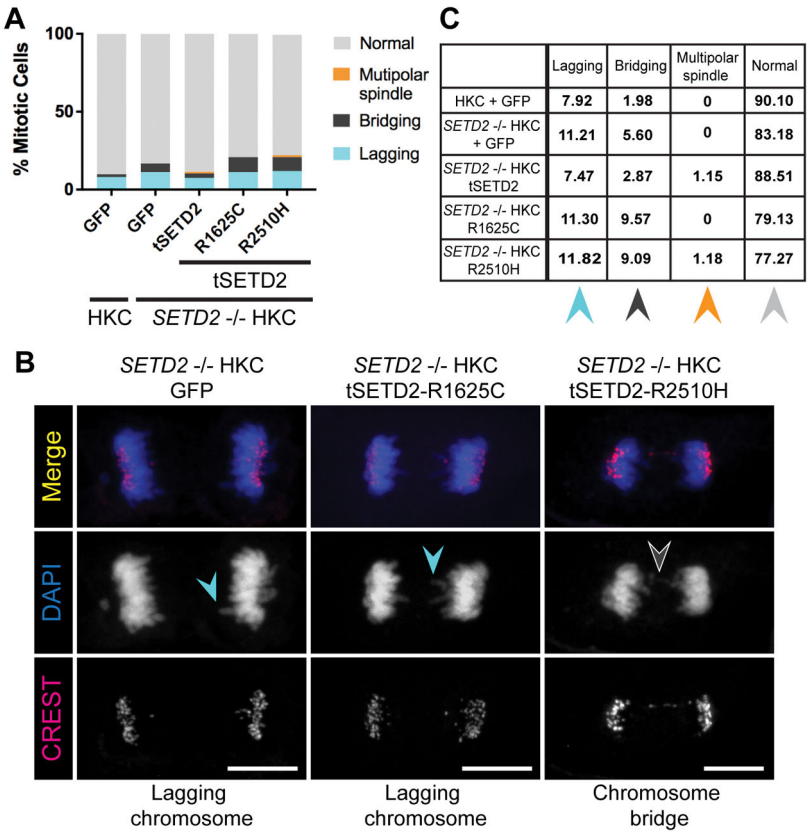

	Lagging	Bridging	Multipolar spindle	Normal
HKC + GFP	7.92	1.98	0	90.10
SETD2 -/- HKC + GFP	11.21	5.60	0	83.18
SETD2 -/- HKC tSETD2	7.47	2.87	1.15	88.51
SETD2 -/- HKC R1625C	11.30	9.57	0	79.13
SETD2 -/- HKC R2510H	11.82	9.09	1.18	77.27

Figure 1. *SETD2* loss and pathogenic mutations in SET and SRI domains promote mitotic defects

A, Mitotic cells were plotted for the entire tSETD2 HKC panel. Percentage (%) of cells undergoing normal (light gray) mitosis, or displaying multipolar spindle (orange), chromosome bridging (dark gray), or chromosome lagging defects are represented. **B**, Representative immunofluorescence images of *SETD2* −/− HKC GFP, *SETD2* −/− HKC tSETD2-R1625C, and *SETD2* −/− HKC tSETD2-R2510H co-stained with DAPI (chromosomes; blue) and CREST (centromeres; magenta) are shown. Light blue arrowheads indicate lagging chromosome. Light gray arrowhead indicates chromosome bridge. Bar: 10um. **C**, Quantitation of cells undergoing normal mitosis or displaying lagging chromosome, bridging, or multipolar spindle defects for all tSETD2 HKC panel.

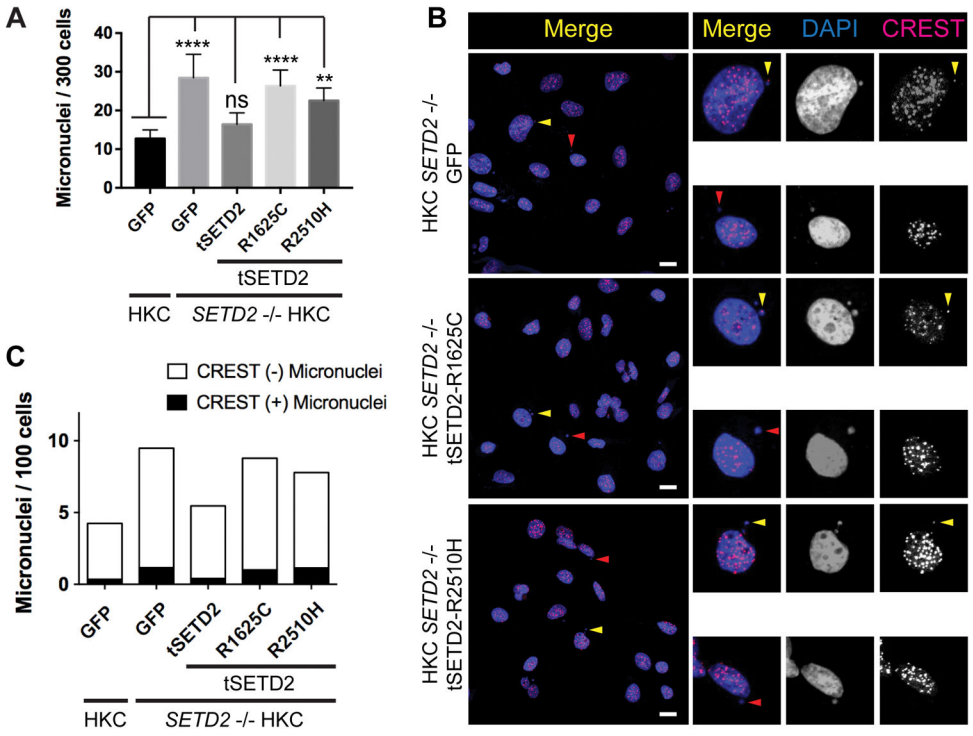

Figure 2. *SETD2* loss and pathogenic mutations in SET and SRI domains promote genomic instability

A, Micronuclei quantitation from entire tSETD2 HKC panel. **, $P < 0.01$; ****, $P < 0.0001$; ns, no statistical significance observed**. B**, Representative immunofluorescence images of *SETD2* −/− HKC GFP, *SETD2* −/− HKC tSETD2-R1625C, and *SETD2* −/− HKC tSETD2-R2510H co-stained with DAPI (nuclei and micronuclei; blue) and CREST (centromeres; magenta) are shown. Yellow arrowheads: DAPI/CREST (+) micronuclei. Red arrowheads: DAPI (+) CREST (−) micronuclei of selected cells magnified (3x digital zoom) in each inset. **C**, Quantitation of CREST (+) and CREST (−) micronuclei per 100 cells for the entire tSETD2 HKC panel.

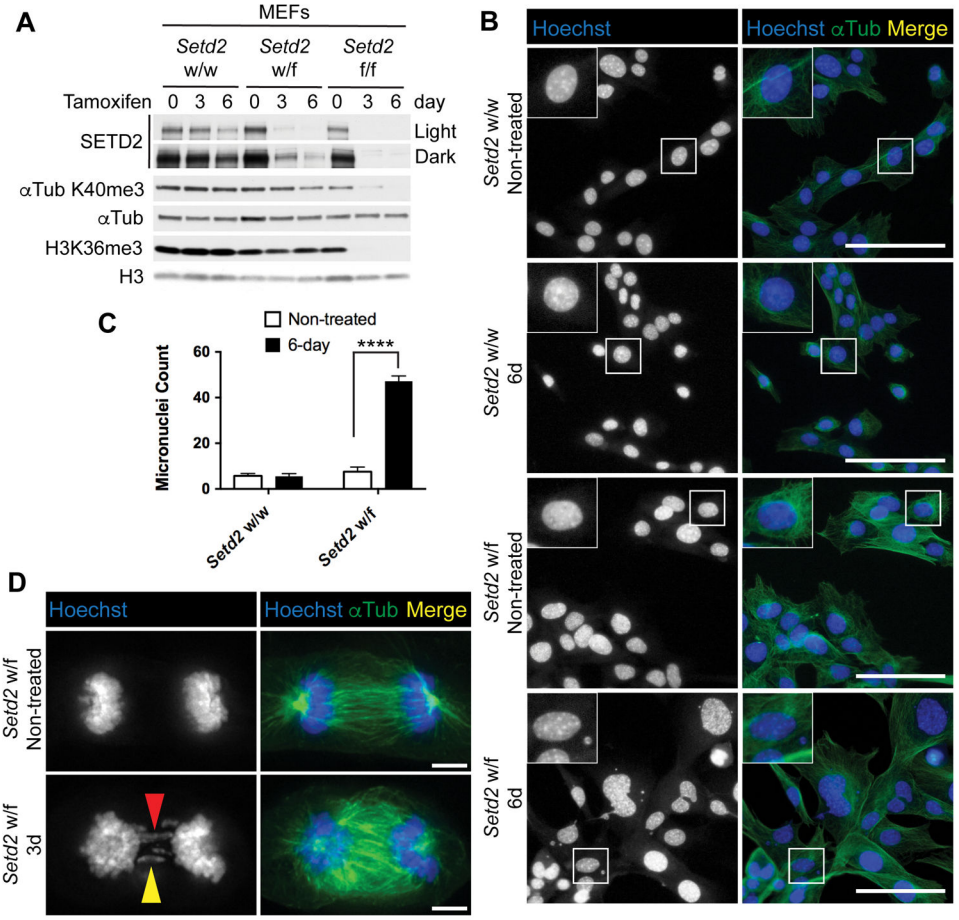

Figure 3. Mono-allelic *SETD2* inactivation is sufficient to lower αTubK40me3 and promote micronuclei formation

A, Western blot analysis of indicated proteins on tamoxifen-treated *Setd2*$^{w/w}$, *Setd2*$^{w/f}$, and *Setd2*$^{f/f}$ MEFs at three different time points (0; 3; and 6 day). Light and dark exposures of SETD2's blots are shown. Histone H3 and αTubulin (αTub) are used as loading controls. **B**, Representative immunofluorescence images of six-day treated (6d) and non-treated *Setd2*$^{w/w}$, and *Setd2*$^{w/f}$ MEFs co-stained with αTubulin (green) and Hoechst (nuclei and micronuclei; blue). Framed cells magnified (3x digital zoom) and Hoechst images shown in insets depicting micronuclei and nuclei. Bar: 100um. **C**, Micronuclei quantitation from six-day treated and non-treated *Setd2*$^{w/w}$, and *Setd2*$^{w/f}$ MEFs shown in panel B. ****, $P < 0.0001$. **D**, Representative immunofluorescence images of three-day (3d) treated and non-treated *Setd2*$^{w/f}$ MEFs co-stained with αTubulin (green) and Hoechst (blue) showing lagging chromosome (yellow arrowhead) and chromosome bridge (red arrowhead). Bar: 10um.

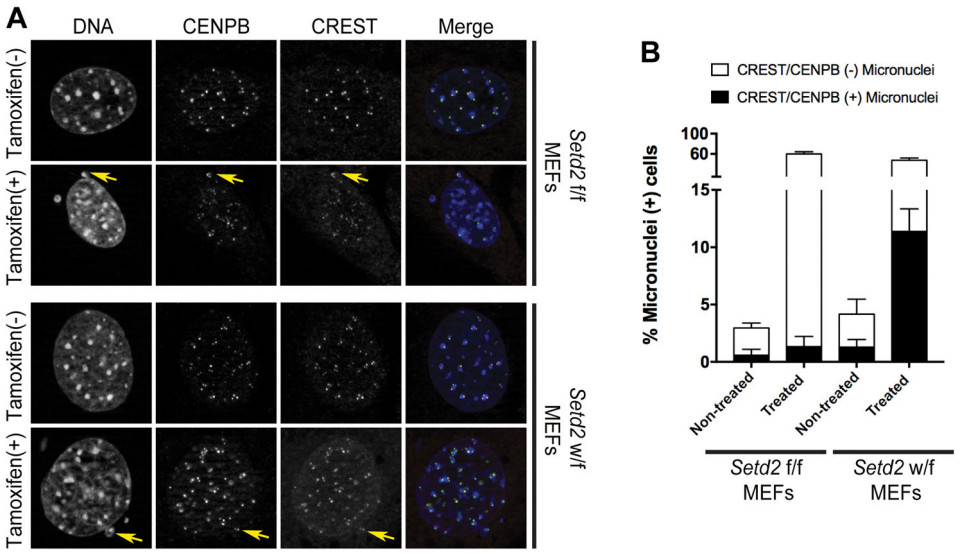

Figure 4. *SETD2* haploinsufficiency promotes genomic instability

A, Representative immunofluorescence images of tamoxifen-treated and non-treated *Setd2*$^{f/f}$ and *Setd2*$^{w/f}$ MEFs co-stained with Hoechst (nuclei and micronuclei), CENPB and CREST (centromeres) are shown. Yellow arrows point to Hoechst/CENPB/CREST (+) staining. **B**, Percentage (%) of micronuclei + cells. Quantitation of CREST (+) (black) and CREST (−) (white) micronuclei within micronuclei (+) cells for *Setd2*$^{f/f}$ and *Setd2*$^{w/f}$ MEFs.

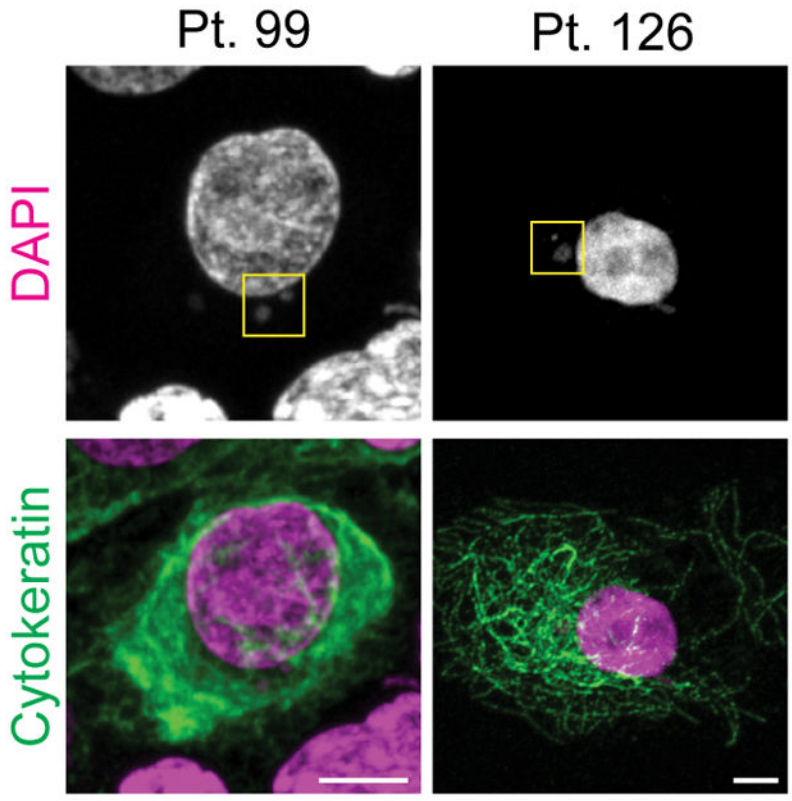

Figure 5. Micronuclei detected in ccRCC patient-derived tumors

Immunofluorescence images of patients 99 and 126 co-stained with DAPI (nuclei and micronuclei; magenta) and cytokeratin (epithelial and tumor cells; green). Yellow boxes enclose micronuclei. Bar: 5um.

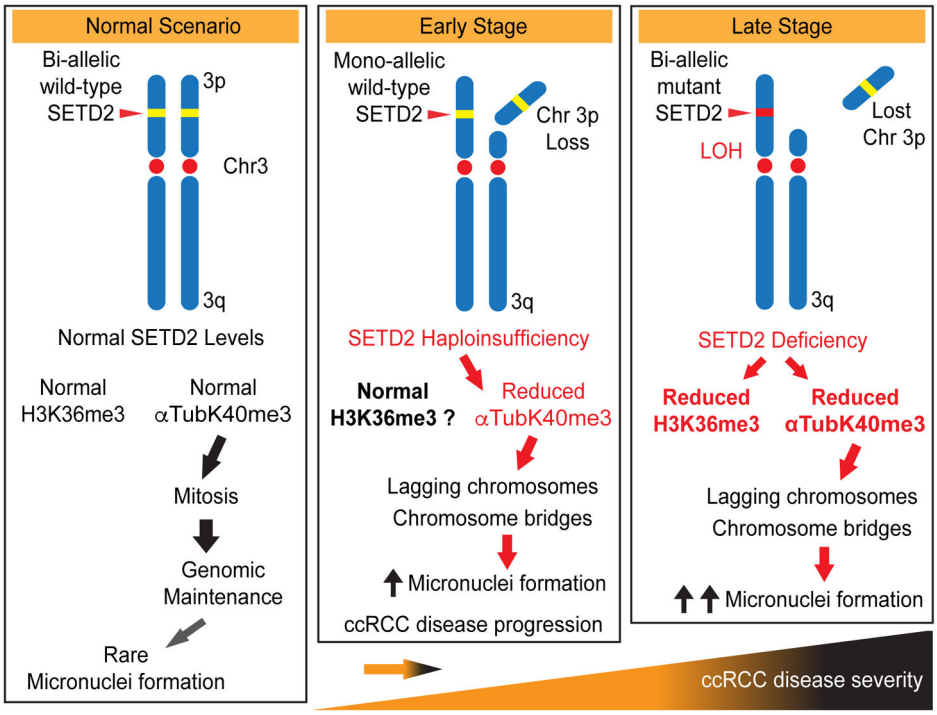

Figure 6. Proposed stepwise model of loss of SETD2 functionality

We postulate that *SETD2* haploinsufficiency during early stages of ccRCC plays a crucial role in the disease progression by reducing αTubK40me3 levels and thus causing genomic instability. At later stages, *SETD2* haploinsufficiency potentially creates conditions conducive to the harsher setting of bi-allelic loss with associated complete loss of trimethylating activity. Yellow rectangle: wild-type *SETD2* gene. Red rectangle: mutated *SETD2* gene.

Table 1

Micronuclei are a feature of ccRCC patient-derived tumors

Quantifying histologic grade, H3K36me3 status, percentage of micronucleated tumor and normal cells according to histology and predicted status of chromosome 3p. Patient 126, and nonclear cell tumors without normal match.

Patient ID	Tumor type	Histologic Grade	% micronucleated tumor cells	% micronucleated normal cells
Chr 3p Loss				
54	ccRCC	G3	1.14 (1/88)	0.00 (0/69)
55	ccRCC	G2	2.67 (2/75)	0.00 (0/59)
91	ccRCC	G2	3.09 (3/90)	1.59 (2/126)
99	ccRCC	G4	1.11 (1/90)	0.00 (0/88)
126	ccRCC	G2	30.3 (10/33)	No matched normal
No Chr 3p Loss				
74	pRCC	G2	0.00 (0/248)	No matched normal
77	pRCC	G2	0.49 (3/608)	No matched normal
65	Oncocytoma	N.R.	0.28 (1/352)	No matched normal
87	Oncocytoma	N.R.	0.20 (1/505)	No matched normal